Part 1: Simulation Studies of Three Tracers for Validation of Impact of Respiratory Motion on Dynamic Analysis

We conducted simulation studies for three different tracers (^{82}Rb, ^{18}F-FP(+)DTBZ and ^{18}F-fluoromisonidazole (FMISO)) to investigate the impact of respiratory motion on dynamic analysis, as no gold standard kinetic parameters could be obtained in human studies.

We simulated respiratory motion for target organs (^{82}Rb: myocardium/blood pool, ^{18}F-FP(+)DTBZ: pancreas; FMISO: lung tumor) based on real human respiratory traces acquired by the Anzai system (Anzai Medical, Tokyo, Japan). Both stress and rest studies were simulated for ^{82}Rb.

The simulated motion-free templates of target organs were extracted without background from NCAT phantom (*1*) for myocardium/left-ventricle (LV) blood pool, and segmentation of real human gated images for pancreas and lung tumor as Supplemental Figure 1A shows.

Thirty-two (3 s × 20, 10 s × 6, 20 s × 6), forty-nine (30 s × 6, 1 min × 3, 2 min × 2, 5 min × 38) and thirty-nine (30 s × 6, 1 min × 3, 2 min × 2, 5 min × 28) dynamic frames were generated respectively for ^{82}Rb, ^{18}F-FP(+)DTBZ and FMISO.

The regional radioactivity assigned for each dynamic frames was calculated from kinetic models (^{82}Rb: 1-tissue model with 3 parameters, ^{18}F-FP(+)DTBZ: 2-tissue model with 4 parameters, FMISO: 2-tissue irreversible model with 4 parameters) with input function extracted from real human data.

For each frame, respiratory motion information was estimated independently. The corresponding Anzai traces within one frame were histogram into 20 bins. The mean value of each bin was taken as the external motion amplitude of one potential motion location. The frequency of the bin corresponds to the respiratory time dwelling at this location. Utilizing the correlation built between internal and external, 3-dimentinal internal motion vectors were generated with the mean value of each bin to guide a rigid transformation of target organ. The weighted average of twenty relocated images was taken as a motion-blurred one (Supplemental Fig. 1B).

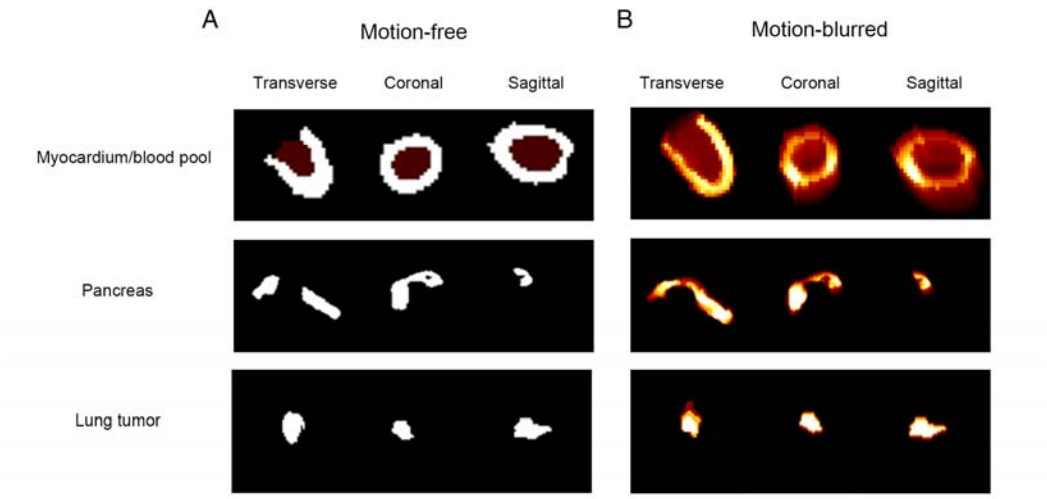

SUPPLEMENTAL FIGURE 1. A) The simulation templates of target organs: NCAT phantom for myocardium/blood pool, and real human gated images for pancreas and lung tumor. B) The simulated motion-blurred images in one dynamic frame.

3D regions of interest (ROI) were defined from motion-blurred PET images based on the level-set segmentation. Time-activity curves (TAC) of the target organ were then obtained. TAC of left-ventricle for ^{82}Rb study was also obtained.

For ^{82}Rb study, K_1 values were obtained with a 1-tissue model using left-ventricle image-derived input function fitted to a 3-parameter model. Myocardial blood flows (MBF) and coronary flow reserve (CFR) were calculated based on previously published ^{82}Rb extraction function equation.

Total volume of distribution (V_T) of the pancreas was estimated with the known input function by the multi-linear analysis 1 method for 18F-FP(+)DTBZ data.

2-tissue irreversible model was used for FMISO with analysis to estimate K_i from $K_1k_3/(k_2+k_3)$ with the known input function.

The data analysis and kinetic modeling for the three tracers were identical to those described in the manuscript. All parameters were compared to the motion-free values.

Supplemental Figure 2(A) and (B) shows sample TACs of myocardium and LV blood pool for both motion-free and motion-blurred analyses in stress/rest ^{82}Rb studies. For stress study with 13.3mm motion amplitude, respiratory motion changed the shape and values of both tissue and blood pool TACs, specifically decreasing the later tissue values and increasing the late blood pool data. For rest study with 5.4 mm motion amplitude, the motion-free and motion-blurred TACs nearly overlapped.

Supplemental Figure 2(C) and (D) show TACs of the pancreas and lung tumor ROIs. Motion blurring results lower uptake in the TACs.

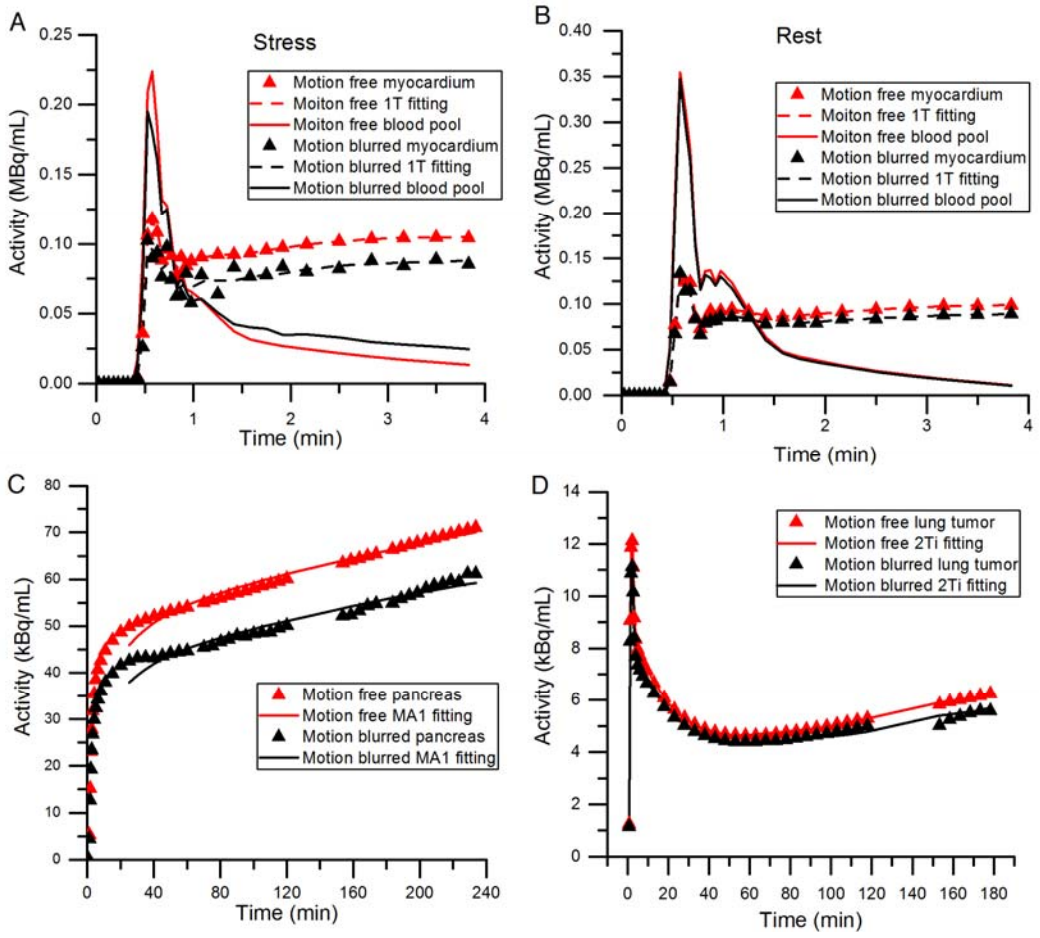

SUPPLEMENTAL FIGURE 2. Time activity curves for both Motion-free and Motion-blurred analyses. Motion-free data are displayed in red and motion-blurred data are in black. The symbols show the ROI values and the solid lines give the fitting result. A) Myocardium and blood pool of left ventricle (stress), B) Myocardium and blood pool of left ventricle (rest), C) pancreas, D) tumor in lung.

As Supplemental Table 1 shows, after simulated respiratory motion blurring, K_1, V_T and K_i were decreased by 18% / 5% (stress / rest), 18% and 17% respectively. For ^{82}Rb studies, MBF decreased by 29% and 8% for stress and rest respectively. CFR decreased by 17%.

This simulation study validated that for three different tracers, respiratory motion resulted in decreased kinetic parameters. With internal motion amplitude and organ template derived from human studies, the trend and magnitude of parameter change in the simulation study are consistent with the *in vivo* human data shown in the manuscript, where INTEX motion correction increased kinetic parameters by similar

percent difference.

SUPPLEMENTAL TABLE 1. K_1, V_T and K_i value for ^{82}Rb, ^{18}F-FP(+)DTBZ and FMISO subjects respectively. Percent difference comparing Motion-free to Motion-blurred results are shown.

Trace	Motion Amplitude (mm)	Kinetic Parameter	Motion-free		Motion-blurred	Percent difference
^{82}Rb	13.3/5.4 Stress/rest	K_1	Stress	1.62	1.37	17.8%
			Rest	0.68	0.65	4.6%
		MBF	Stress	5.06	4.00	26.5%
			Rest	1.29	1.19	8.4%
		CFR	3.92		3.36	16.7%
^{18}F-FP(+)DTBZ	10.3	V_T	175.1		148.6	17.8%
FMISO	5.2	K_i	0.0042		0.0036	16.7%

Part 2: Internal-external motion correlation in one dynamic scan

INTEX respiratory motion correction relies on linear correlations between internal organ motion and measured external motion. Previous study has demonstrated that the correlation between internal and external might change for every 10 minutes (*2*). To investigate the impact of time-dependent correlation change on motion correction, correlations built from four 10-min frames and 1 40-min frame of Subject 8 were investigated as an example.

The slopes and coefficients (*R*) of each correlation are listed in Supplemental Table 2. Using slopes built from corresponding individual 10-min frame (self-correlation) and 40-min frame (global-correlation), we generated two motion files to correct motion respectively for every 10 minutes. Percent-differences of the regional activity of pancreas reconstructed with and without motion correction were calculated for each correlation. The difference of regional concentration improvements after motion correction is less than 3% between using global correlation and self-correlations. Therefore, we do not expect the time-dependent INTEX correlation change will substantially affect our results, though slightly more accurate results might be reached if self-correlations could be built for every 10 minutes. So in this study, we directly extended the correlation built from first 30-minutes frames to the entire respiratory recording period for Subject# 8-12. For cardiac studies (Subject# 1-7), we built correlation based on data from 2-6 min post injection and extended it to the first 2 min data.

SUPPLEMENTAL TABLE 2. Slope and coefficient (R) of correlations in the anterior-posterior (AP) and superior-inferior (SI) directions built based on four 10-min and one 40 min frames of Subject# 9. Percent difference of activity in pancreas with/without motion correction using both global-correlation and self-correlation are listed.

t/min	anterior-posterior (AP) direction		superior-inferior (SI) direction		Activity-difference(ROI)	
	slope	R	slope	R	Global-correlation	Self-correlation
[0 ,10]	0.058	0.98	0.12	0.98	10.9%	13.6%
[10,20]	0.046	0.99	0.12	0.98	13.7%	16.3%
[20,30]	0.031	0.97	0.09	0.96	8.3%	6.8%
[30,40]	0.026	0.96	0.07	0.98	5.4%	3.5%
[0 ,40]	0.042	0.86	0.11	0.89		

Part 3: Sizes of 3D regions of interest

SUPPLEMENTAL TABLE 3. A list of all 3-dimentional ROI defined to calculate the regional radioactivity of target organs (Subject #1-7: myocardium, Subject #8-11: pancreas, Subject #12: tumor in lung). The sizes of ROI for left-ventricle blood pool in ^{82}Rb studies are also listed.

Subject Number	Tracer	Region of Interest (ROI)	Size of ROI (number of voxels)	
			STRESS	REST
1	^{82}Rb	Myocardium	1573	1342
		LV blood pool	130	158
2	^{82}Rb	Myocardium	1461	1640
		LV blood pool	207	179
3	^{82}Rb	Myocardium	1298	1493
		LV blood pool	184	207
4	^{82}Rb	Myocardium	1682	2284
		LV blood pool	134	188
5	^{82}Rb	Myocardium	1572	1385
		LV blood pool	231	169
6	^{82}Rb	Myocardium	1297	978
		LV blood pool	154	198
7	^{82}Rb	Myocardium	1254	1455
		LV blood pool	216	177
8	^{18}F-FP(+)DTBZ	Pancreas	5392	
9	^{18}F-FP(+)DTBZ	Pancreas	4470	
10	^{18}F-FP(+)DTBZ	Pancreas	3632	
11	^{18}F-FP(+)DTBZ	Pancreas	7488	
12	FMISO	Lung tumor	1666	

Part 4: Internal-external motion correlations in both stress and rest studies for one subject

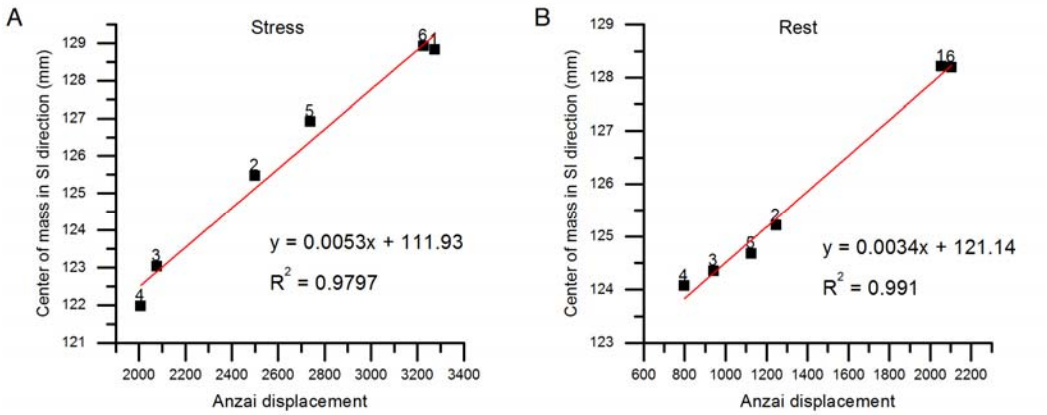

SUPPLEMENTAL FIGURE 3. Linear correlations between the internal motion of myocardium in SI direction and the external respiratory signals in 6 respiratory gates for one subject during both regadenosine induced stress(A) and rest(B) imaging with ^{82}Rb.

References

1. Segars WP, Tsui B, Lalush D, Frey E, King M, Manocha D. Development and application of the new dynamic Nurbs-based Cardiac-Torso (NCAT) phantom. 2001.

2. Malinowski K, McAvoy TJ, George R, Dietrich S, D'Souza WD. Incidence of changes in respiration-induced tumor motion and its relationship with respiratory surrogates during individual treatment fractions. *INT J RADIAT ONCOL*. 2012;82:1665-1673.